RESEARCH ARTICLE

Distinct CED-10/Rac1 domains confer context-specific functions in development

Steffen Nørgaard[1,2◉], Shuer Deng[1◉], Wei Cao[1], Roger Pocock[1,2]*

1 Development and Stem Cells Program, Monash Biomedicine Discovery Institute and Department of Anatomy and Developmental Biology, Monash University, Melbourne, Victoria, Australia, **2** Biotech Research and Innovation Centre, University of Copenhagen, Copenhagen, Denmark

◉ These authors contributed equally to this work.
* roger.pocock@monash.edu

Abstract

Rac GTPases act as master switches to coordinate multiple interweaved signaling pathways. A major function for Rac GTPases is to control neurite development by influencing downstream effector molecules and pathways. In *Caenorhabditis elegans*, the Rac proteins CED-10, RAC-2 and MIG-2 act in parallel to control axon outgrowth and guidance. Here, we have identified a single glycine residue in the CED-10/Rac1 Switch 1 region that confers a non-redundant function in axon outgrowth but not guidance. Mutation of this glycine to glutamic acid (G30E) reduces GTP binding and inhibits axon outgrowth but does not affect other canonical CED-10 functions. This demonstrates previously unappreciated domain-specific functions within the CED-10 protein. Further, we reveal that when CED-10 function is diminished, the adaptor protein NAB-1 (Neurabin) and its interacting partner SYD-1 (Rho-GAP-like protein) can act as inhibitors of axon outgrowth. Together, we reveal that specific domains and residues within Rac GTPases can confer context-dependent functions during animal development.

Author summary

Brain development requires that neurite outgrowth and guidance are precisely regulated. Previous studies have shown that molecular switch proteins called Rac GTPases perform redundant functions in controlling neurite development. Using a pair of bilateral neurons in the nematode *Caenorhabditis elegans* to model neurite development, we found that a single amino acid in a conserved domain of the Rac GTPase CED-10 is crucial for controlling neurite outgrowth in a partially non-redundant manner. Further, we revealed that lesions in discrete domains in the CED-10 protein lead to distinct developmental defects. Therefore, our *in vivo* study proposes that regulation of distinct signalling pathways through Rac GTPase protein domains can drive different developmental outcomes.

Introduction

Correct axonal projection is essential for developing a functional nervous system. The *Caenorhabditis elegans* ventral nerve cord (VNC) contains two fascicles housing multiple neurons

that project axons along the length of the animal [1]. During development, the extending tips of VNC axons (growth cones) facilitate faithful navigation of their environment by interpreting outgrowth and guidance signals [2–10]. Growth cones assimilate molecular information from neighbouring cells and the extracellular environment through ligand-receptor interactions. Receptors then regulate complex and interconnected intracellular signaling cascades that ultimately control cytoskeletal dynamics [11, 12]. These signalling mechanisms are tightly orchestrated, both temporally and spatially, to ensure precise nervous system development.

Rho GTPase family members (Rho, Rac and Cdc42) are key regulators of actin cytoskeletal dynamics [13], and are especially recognized for their role in regulating axon outgrowth and guidance [14, 15]. The three *C. elegans* Rac GTPases, CED-10, MIG-2 and RAC-2 have overlapping functions in the context of axon outgrowth and guidance [16]. As such, classical single mutants in any of the *C. elegans* Rac GTPases result in minor axonal defects with compound mutations having synergistic effects on outgrowth and guidance [16]. A major function for Rac GTPases is to coordinate actin filament networks at the growth cone of an extending axon [17, 18]. Actin filaments deliver mechanical support to the growth cone that enables force to generate movement. As such, protrusive activity (outgrowth) of an axon through a complex extracellular environment requires actin cytoskeletal remodeling. This highly regulated and complex process requires more than 100 accessory proteins to control the balance between actin filament elongation and branching. Rac GTPases act as master switches during actin cytoskeletal remodeling, acting upstream of both actin elongation drivers such as Ena/VASP and actin branching drivers such as the Arp2/3 complex [13].

The Rac GTPase, Rac1, harbors several major functional domains that are highly conserved in metazoa: the guanine-binding domains, the membrane-targeting region, and Switch 1 and 2 regions. The guanine-binding domains bind guanosine diphosphate (GDP) or guanosine triphosphate (GTP), and the guanine-binding status determines whether Rac1 is inactive (GDP-bound) or active (GTP-bound). The membrane-targeting region of Rac1 is prenylated at specific amino acids to direct the protein to the plasma membrane, its site of action [19]. Finally, the Switch 1 and 2 regions are important for coordinating interactions that the Rac GTPase forms with regulatory and effector molecules. The Rac GTPase activity status can induce conformation changes in the Switch 1 and 2 regions that specify which regulatory or effector molecule it interacts with [20, 21]. Therefore, Rac GTPase activity modulates the output of this molecular switch. Two major types of upstream regulators control Rac GTPase activation status. Guanine nucleotide exchange factors (GEFs) exchange bound GDP for GTP, thereby activating Rac GTPases; and GTPase-activating proteins (GAPs) inactivate Rac GTPases by enhancing their intrinsic GTPase activity [22, 23].

Here, we identified a genetic lesion, *ced-10(rp100),* that causes axon guidance and outgrowth defects in the PVQ VNC interneurons in *C. elegans*. The dramatic outgrowth defects observed in the *ced-10(rp100)* strain are caused by a single amino acid substitution (G30E) in the Switch 1 region of the CED-10 protein. We demonstrate that *ced-10(rp100)* acts recessively and a G30E substitution causes reduced GTP binding to Rac1 protein *in vitro*. In contrast, other viable mutations in CED-10, which have genetic lesions in the Switch 2 region (G60R) or the membrane-targeting region (V190G), exhibit PVQ axon guidance defects but do not show PVQ outgrowth defects. Further, CED-10(G30E) animals do not present canonical phenotypes caused by the G60R and V190G mutations—such as low brood size and the accumulation of apoptotic cell corpses. This posits that mutant CED-10(G30E) protein adversely affects specific downstream neuronal pathways while leaving non-neuronal functions intact. Our data also demonstrate that there are domain-specific CED-10 functions that can confer context-dependent roles during animal development.

In an unbiased genetic modifier screen, we identified that NAB-1 (Neurabin homolog) and SYD-1 (RhoGAP-like), a known NAB-1-interacting protein, inhibit PVQ outgrowth in

animals with reduced CED-10 function. This suggests that NAB-1 and SYD-1 inhibit Rac GTPase activity to control axon outgrowth through GAP-dependent inhibition. Together, this study delineates regulatory functions of Rac GTPases and conceptualizes how different domains exhibit tissue-specific regulatory functions during development.

Results

A mutation in the CED-10/Rac1 Switch 1 region causes defects in axon outgrowth and guidance

During embryogenesis, the PVQL/R interneurons project axons from the tail into the ipsilateral fascicle of the ventral nerve cord (VNC) and terminate at the nerve ring in the head (Fig 1A).
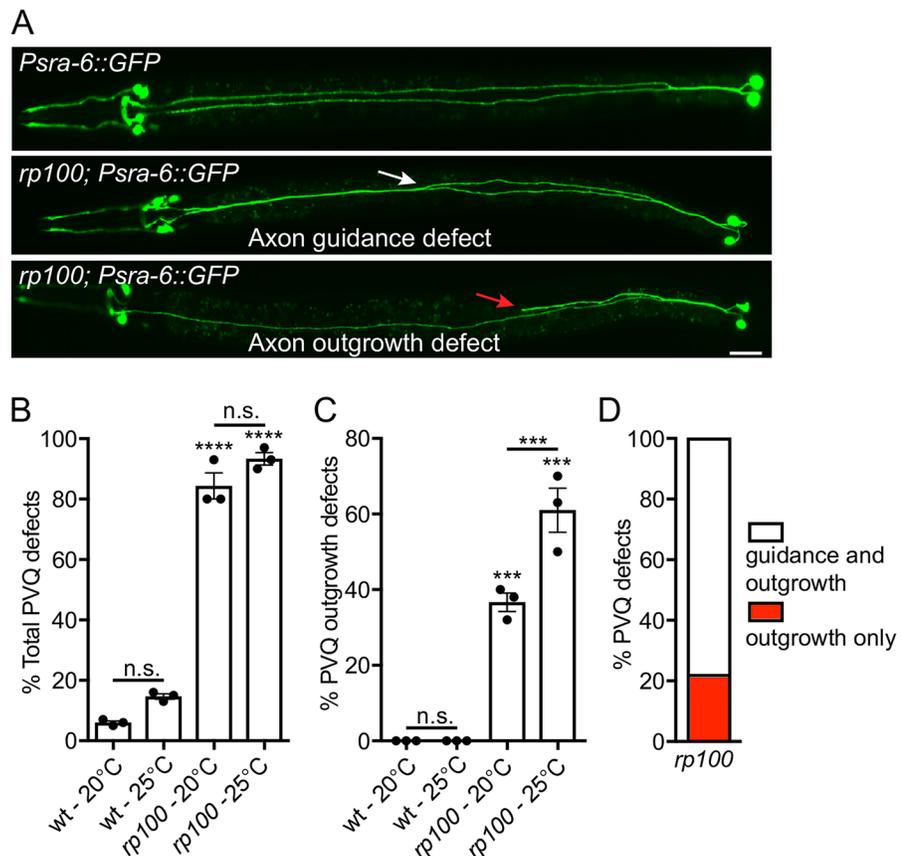
Fig 1. A spontaneous mutation causes severe defects in PVQ development. (A) Ventral views of animals expressing the transgene *Psra-6::gfp* to visualize the anatomy of the PVQ neurons (PVQL and PVQR). In wild type adult animals (upper image), the PVQ axons extend axons from the posterior into the ipsilateral side of the VNC. In *rp100* animals, PVQ axons inappropriately cross to the contralateral side of the VNC (middle image, white arrow) and/or exhibit premature termination of outgrowth (lower image, red arrow). Posterior to the right. Scale bar 20 μm.(B) The *rp100* genetic lesion causes highly penetrant defects in PVQ development.Wild type and *rp100* animals were incubated at 20°C or 25°C. Data are expressed as mean ±SD and statistical significance was assessed using t test. ****<0.0001, comparing wild type and *rp100* animals, n.s. not statistically significant. n = 90 per strain, each dot represents independent scoring replicates.(C) The *rp100* genetic lesion causes highly penetrant, and temperature-sensitive, defects in PVQ axon outgrowth. The position of outgrowth defects was randomly distributed along the anterior-posterior axis. Wild type and *rp100* animals were incubated at 20°C or 25°C. Data are expressed as mean ±SD and statistical significance was assessed using t test. ***<0.001, comparing wild type and *rp100* animals or *rp100* incubated at 20°C and 25°C, n.s. not statistically significant. n = 90 per strain, each dot represents independent scoring replicates.(D) Phenotypic classification of PVQ outgrowth defects in *rp100* animals at 20°C. Approximately 80% of animals with outgrowth defects also have guidance defects (white bar) and 20% of outgrowth defects occur independently of a guidance defect (red bar). n = 90, over three independent scorings.

We identified a spontaneous mutation, called *rp100*, which causes over 80% penetrant defects in PVQ development (Fig 1A and 1B). Specifically, *rp100* causes the PVQ neurons to be inappropriately guided to the contralateral side of the ventral nerve cord and causes premature termination of the PVQ neurons (Fig 1A–1D). Elevated temperature is known to place an added burden on axonal development, potentially due to accelerated development and/or perturbation of signaling pathways. Therefore, we examined how temperature effects PVQ development in *rp100* mutant animals at 20˚C or 25˚C. We found that the PVQ outgrowth defects of *rp100* mutant animals increased from ~35% to ~60% when raised at 25˚C (Fig 1C), indicating that increased temperature enhances the detrimental effects of the *rp100* mutation on PVQ development. We wished to distinguish whether the PVQ axon outgrowth defects are an inherent deficiency in outgrowth or whether they are a secondary consequence of defective guidance. To examine this, we asked whether outgrowth defects are always accompanied with a guidance defect. We observed that ~20% of the outgrowth defects were not associated with a detectable guidance defect (Fig 1D), implying that the *rp100* mutation affects a fundamental process required for axon outgrowth. To determine if the PVQ axonal defects observed in *rp100* mutant animals are developmental or due to defective maintenance of neuronal architecture, we examined L1 larvae raised at 20˚C and found that the total PVQ defects (88%) and PVQ outgrowth defects (37%) are comparable to those observed in L4 larvae (Fig 1B and 1C), indicating that *rp100* causes defects in axonal development.
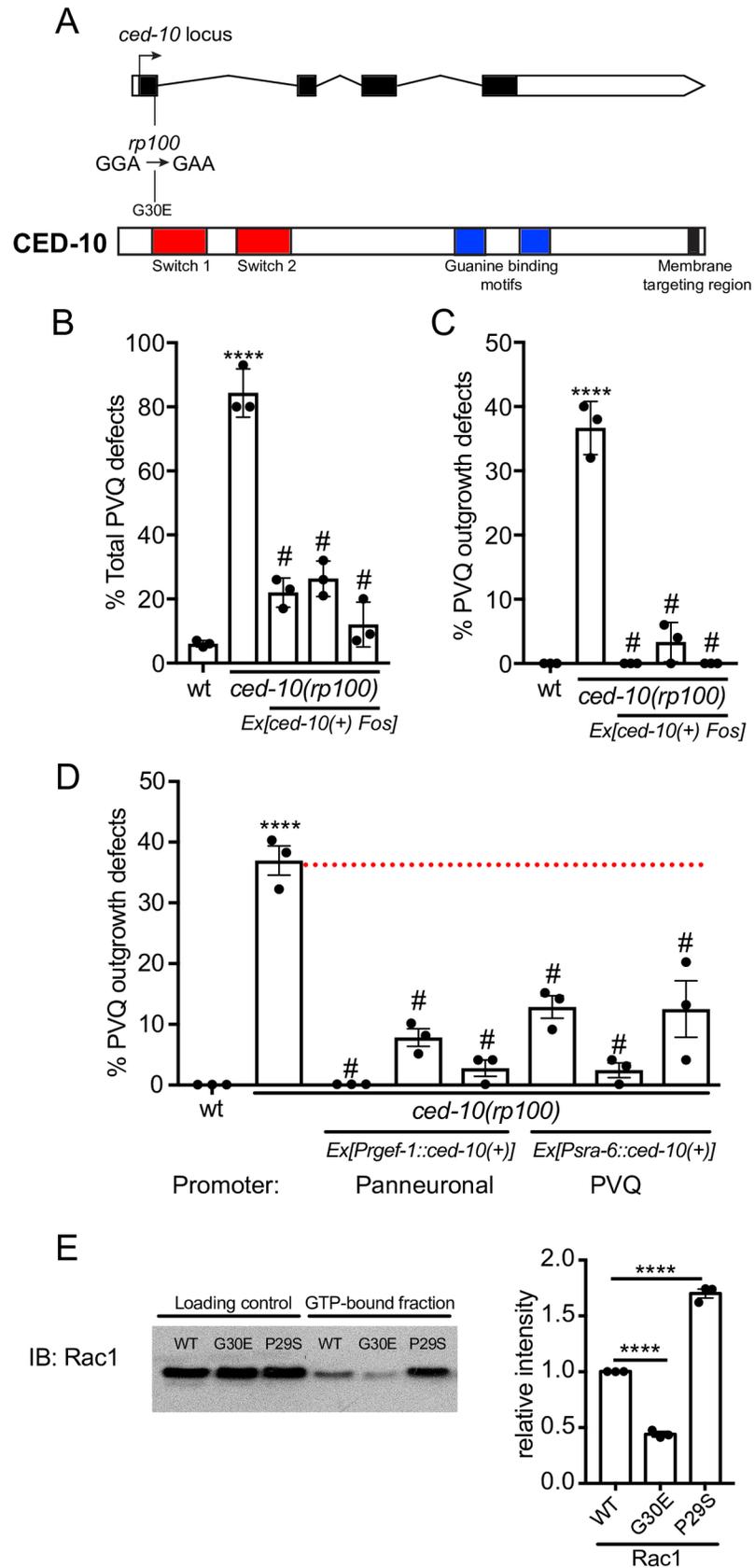
To determine the molecular identity of the *rp100* genetic lesion we used a one-step whole-genome sequencing and SNP mapping method [24]. We found that *rp100* is a missense mutation, which results in an amino acid substitution from glycine (G) to glutamic acid (E) at position 30 in the Rac GTPase homolog CED-10 (Figs 2A and S1A). We confirmed that *ced-10 (rp100)* causes PVQ outgrowth and guidance defects by rescuing both phenotypes through transgenic expression of a fosmid containing the *ced-10* locus (Fig 2B and 2C).

CED-10 acts cell-autonomously to control PVQ development

Rac GTPases are key regulators of cytoskeletal dynamics at the growth cone. As such, CED-10 is likely to act cell-autonomously to control PVQ axon outgrowth and guidance. To examine this, we expressed *ced-10* cDNA in the *ced-10(rp100)* strain using either the *rgef-1* promoter for pan-neuronal expression, or the *sra-6* promoter for PVQ-specific expression. We found that pan-neuronal and PVQ-specific *ced-10* expression robustly rescued PVQ outgrowth defects and partially rescued PVQ guidance defects (Fig 2D and S1B Fig). Incomplete rescue of PVQ guidance defects could be due to inappropriate timing or level of *ced-10* expression using these heterologous promoters. Nonetheless, the sub-optimal cell-autonomous rescue of PVQ defects prompted us to perform mosaic analysis to confirm our rescue data (S1C Fig). We transgenically expressed *ced-10* cDNA pan-neuronally and then identified rare mosaic animals that lost the extrachromosomal rescuing array in the PVQ neurons. Here we found that *ced-10* expression in the PVQ neurons is required for PVQ axon outgrowth and guidance (S1C Fig). Therefore, we conclude that CED-10 acts cell autonomously to regulate PVQ axon outgrowth and guidance.

ced-10(rp100) is a hypomorphic allele

The glycine affected by the G30E substitution is situated at the N-terminus of the Switch 1 region, a region fully conserved between CED-10 and Rac1 (Figs 2A and S1A). The Switch 1 region is known to coordinate interactions with upstream regulatory and downstream effector molecules [25]. Another mutation associated with the Switch 1 region, Rac1(P29S) causes gain-of-function effects to Rac GTPases (excessive GTP binding) [26]. Therefore, we used a

A

ced-10 locus

rp100
GGA → GAA

G30E

CED-10

Switch 1   Switch 2   Guanine binding   Membrane
                             motifs   targeting region

B

C

D

Promoter: Panneuronal   PVQ

E

IB: Rac1

Fig 2. *rp100* is a mutation in the Switch 1 region of CED-10/Rac1. (A) Molecular identification of *rp100* as an allele of *ced-10*. *ced-10(rp100)* is a missense mutation in the first exon (GGA-GAA), causing a substitution of glycine at position 30 for a glutamic acid in the Switch 1 region of the Rac GTPase CED-10. The conserved domains within CED-10/Rac1 are marked as follows: Switch 1 and 2 regions (red boxes), guanine binding motifs (blue boxes) and membrane targeting region (black box). See S1A Fig for full sequence conservation between *C. elegans* CED-10 and human Rac1.(B-C) Transgenic expression of a fosmid containing the *ced-10* locus (WRM0639dH09) rescues both total PVQ defects (B) and outgrowth defects (C) of *ced-10(rp100)* animals. ****<0.0001, comparing wild type and *ced-10 (rp100)* animals; #<0.0001 comparing the three transgenic rescue lines to *ced-10(rp100)*. n = 90 per strain, each dot represents independent scoring replicates.(D) Transgenic expression of *ced-10* cDNA controlled by a pan-neuronal (*Prgef-1*) or PVQ-specific (*Psra-6*) promoter rescues PVQ outgrowth defects of *ced-10(rp100)* animals. Data are expressed as mean ±SD and statistical significance was assessed using one-way ANOVA, with Tukey's multiple comparison test. ****<0.0001, comparing wild type and *ced-10(rp100)* animals; #<0.0001 comparing the three transgenic rescue lines to *ced-10(rp100)*. n = 90 per strain, each dot represents independent scoring replicates.(E) *In vitro* pull-down of GTPγS-loaded recombinant Rac1 (wild type, G30E mutant or P29S mutant) with the GTPase-binding domain of PAK1. First three lanes = loading controls. Second three lanes = PAK1 binding assay to detect the GTP-bound fraction. Rac1(G30E) protein exhibits weaker PAK1 binding compared to wild type Rac1. The Rac1(P29S) gain-of-function mutant control shows excess PAK1 binding, as described previously [26]. Quantification of three independent experiments is shown in the graph. Data are expressed as mean ±SD and statistical significance was assessed using one-way ANOVA, with Tukey's multiple comparison test. ****<0.0001, comparing each Rac1 mutant protein to wild type.

https://doi.org/10.1371/journal.pgen.1007670.g002

combination of genetics and *in vitro* activity assays to ask whether 1) *ced-10(rp100)* acts as a gain- or loss-of-function mutation, 2) the G30E substitution affects the activity of the protein and 3) a known CED-10 gain-of-function mutation can cause PVQ axon outgrowth defects.

First, we examined whether *ced-10(rp100)* acts recessively by crossing a wild type chromosome into the homozygous mutant. We found that *ced-10(rp100)*/+ heterozygotes resemble wild type animals for both PVQ outgrowth and guidance, therefore the *rp100* mutation is recessive (S2A and S2B Fig). Next, we analysed PVQ outgrowth in the balanced *ced-10(tm597)* maternal-effect null allele. The majority of *ced-10(tm597)* animals derived from homozygous mothers die as embryos, however we identified L1 escapers, thereby enabling analysis of PVQ neuroanatomy (S2C Fig). We found that surviving *ced-10(tm597)* L1s exhibit ~60% outgrowth defects, indicating that defects in PVQ outgrowth is a *ced-10* loss-of-function phenotype (S2C Fig).

The activation status of Rac GTPases can affect their ability to regulate downstream signaling pathways during axon outgrowth [27]. Using the Rac1 protein as a model, we tested whether the G30E mutation alters the ability of Rac1 to exchange GDP for GTP. To assay the ability of wild type and mutant Rac1 GTPases to perform nucleotide exchange, we *in vitro* loaded recombinant Rac1-GDP with a non-hydrolyzable GTP analog. Then, we used beads conjugated to p21-binding domain (PDB) of the Rac effector protein p21 activated kinase (PAK) to pull down the Rac1-GTP protein (Fig 2E). PAK-PDB binds with high specificity and affinity to Rac GTPases that are GTP-bound and not GDP-bound [28]. Our quantification of PAK-PDB-bound Rac1 revealed that, as previously reported, PAK-PDB pulled down a higher fraction of the Rac1(P29S) gain-of-function mutant protein than wild type Rac1 [26] (Fig 2E). In contrast, a lower fraction of Rac1(G30E) was pulled down with PAK-PDB beads than wild-type Rac1, suggesting that less Rac1(G30E) protein is GTP-bound after *in vitro* loading compared to wild type Rac1 (Fig 2E).

Next, we used CRISPR Cas9 genome editing to introduce the fast cycling gain-of-function mutation (P29S) into the CED-10 protein and examined PVQ development [26, 29]. We found that animals expressing CED-10(P29S) exhibit 20% PVQ axon guidance defects and 0% axon outgrowth defects (n = 90). Therefore, a known gain-of-function mutation does not have a strong deleterious effect on PVQ development. Together, these data support our genetic experiments showing that the *ced-10(rp100)* mutation causes a partial loss of CED-10 function.

## CED-10(G30E) acts in parallel with MIG-2 to control PVQ outgrowth

The GEF proteins UNC-73/Trio and TIAM-1 are known to positively regulate Rac GTPase activity in the *C. elegans* nervous system [27, 30]. We analysed PVQ development in *unc-73 (e936)* and *tiam-1(ok772)* mutant animals and found that loss of *unc-73*, but not *tiam-1*, results in PVQ outgrowth defects (S1 Table). Moreover, the *unc-73(e936); ced-10(rp100)* double mutant does not exhibit a synergistic effect on axon outgrowth (S1 Table). These data indicate that UNC-73 is the major GEF for CED-10 during PVQ development. Modulating the affinity of GEFs for Rac proteins can fine-tune Rac activity. For example, the neuronal Navigator 1 protein NAV1 binds to Trio, which enhances the affinity of Trio for Rac1, a regulatory mechanism needed to control neurite outgrowth in mammals [31]. In agreement with this, we found that UNC-53, the *C. elegans* homolog of Navigator proteins, is also required for PVQ axon outgrowth (S1 Table). Thus, it is likely that UNC-53 and UNC-73 act upstream of CED-10 to regulate axon outgrowth.

Losing the function of the Rac GTPase regulators UNC-73 and UNC-53 causes outgrowth defects of higher penetrance (55% and 88%, respectively) than observed for *ced-10(rp100)* (37%). This suggests that other Rac GTPases may be activated by UNC-73 to control PVQ outgrowth. Two possible candidates are RAC-2, which is nearly identical in sequence to CED-10, and MIG-2, which is functionally similar to mammalian RhoG [32]. We therefore examined PVQ development in *rac-2(ok326)* and *mig-2(mu28)* mutant animals. We found *rac-2(ok326)* animals are comparable to wild type. However, we observed extensive guidance defects (66%) and minimal outgrowth defects (4%) in the *mig-2(mu28)* null mutant (S1 Table). To ask whether these Rac GTPases act in parallel to CED-10 to control PVQ outgrowth we performed double mutant analysis. We found that *ced-10(rp100); mig-2(mu28)* double mutant animals have highly penetrant defects in PVQ outgrowth (73%) and guidance (100%), whereas the *ced-10(rp100); rac-2(ok326)* is not significantly different from *ced-10(rp100)* (S1 Table). In addition, *ced-10(rp100); mig-2(mu28)* mutant animals are severely uncoordinated, a phenotype not observed in either single mutant. Thus, our data indicate that, as reported previously, multiple neurodevelopmental decisions are redundantly regulated by these Rac GTPases [16, 30].

A previous study showed that the SRGP-1 GTPase activating protein (GAP) negatively regulates CED-10 in the context of apoptotic cell corpse removal [33]. We asked whether SRGP-1 can also act as a GAP in the nervous system by examining PVQ development in the *srgp-1 (gk3017); ced-10(rp100)* double mutant. We observed that loss of SRGP-1 function reduces the PVQ axon outgrowth defects observed in *ced-10(rp100)* animals (S1 Table). Together, these data suggest that upstream activators of Rac GTPase activity, UNC-53, UNC-73 and SRGP-1, control PVQ axon outgrowth through parallel CED-10 and MIG-2 pathways.

PVQ outgrowth defects are specific to the CED-10(G30E) mutation

Null mutations in *ced-10* cause embryonic lethality in *C. elegans* [16]. Therefore, hypomorphic alleles have traditionally been used to decipher biological functions for this Rac GTPase. *ced-10* alleles were originally isolated in genetic screens for mutants that are unable to execute apoptotic corpse engulfment [34, 35]. It was further shown that CED-10 acts in engulfing cells to coordinate cytoskeletal remodeling required for engulfment [36]. Two viable alleles isolated from these screens, *n3246* and *n1993*, affect the Switch 2 (G60R) and membrane targeting regions (V190G), respectively (Fig 3A). We asked whether these amino acid substitutions cause defects in CED-10 function that are important for PVQ development. We observed significant defects in PVQ axon guidance in the *n3246* (~80%) and *n1993* (~40%) *ced-10* alleles (Fig 3B). However, unlike the *rp100* allele, the *n3246* and *n1993* mutations do not cause defects in PVQ outgrowth (Fig 3C). We next performed extensive genetic analysis to delineate the
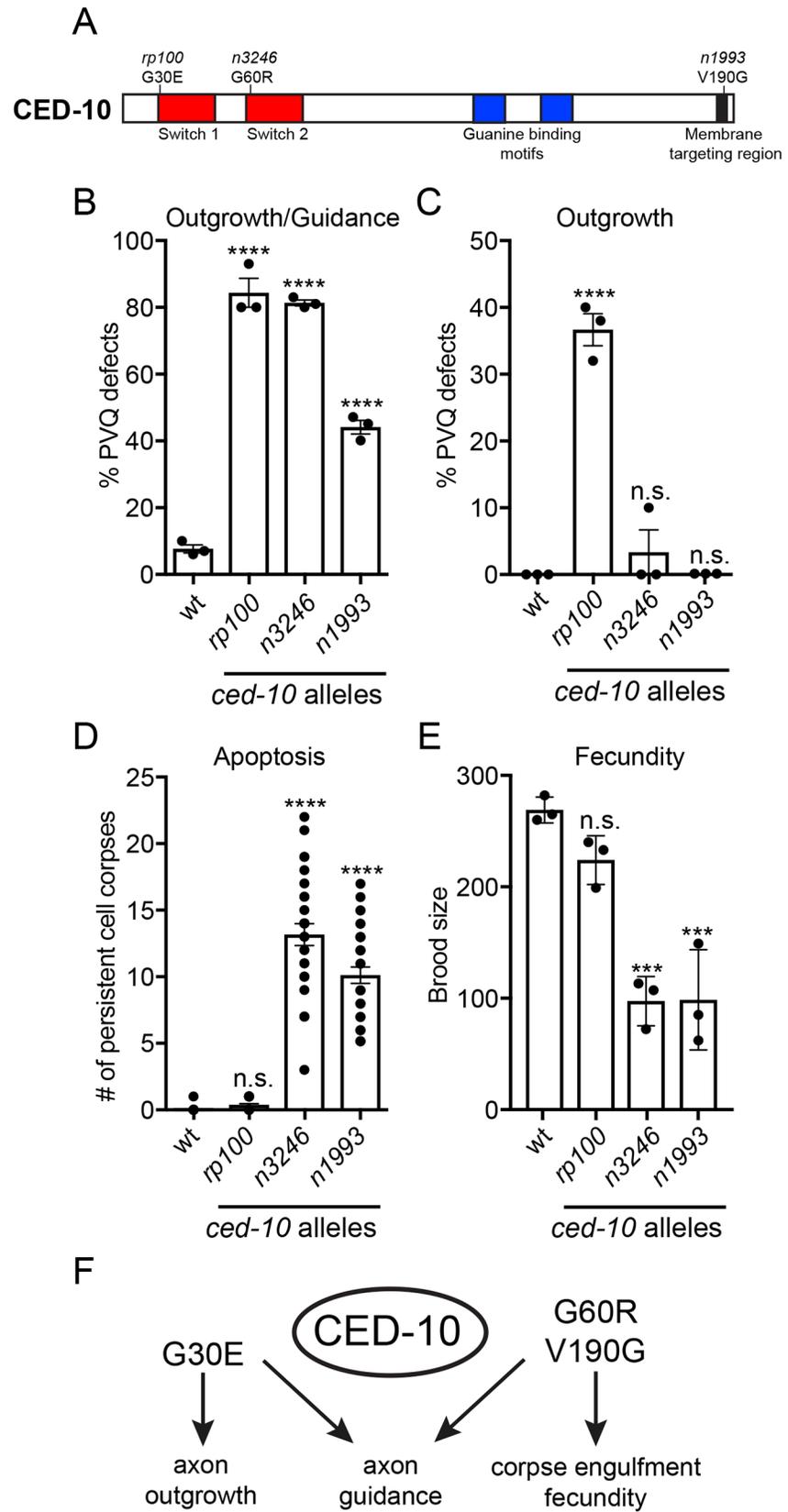
Fig 3. Context-specific effects of *ced-10* alleles. (A) Protein domain structure of CED-10 showing the hypomorphic alleles used in our analysis that affect specific domains. *rp100*(G30E): Switch 1 region; *n3246*(G60R): Switch 2 region and *n1993*(V190G): Membrane-targeting region.(B) All *ced-10* mutant alleles exhibit defects in PVQ development. Data are expressed as mean ±SD and statistical significance was assessed using one-way ANOVA, with Tukey's multiple comparison test. ****<0.0001, comparing *ced-10* alleles to wild type animals. n = 90 per strain, each dot represents independent scoring replicates.(C) Only *ced-10(rp100)*, and not the *n3246* and *n1993* alleles, exhibit PVQ outgrowth defects. Data are expressed as mean ±SD and statistical significance was assessed using one-way ANOVA, with Tukey's multiple comparison test. ****<0.0001, n.s. not statistically significant comparing *ced-10* alleles to wild type animals. n = 90 per strain, each dot represents independent scoring replicates.(D) Persistent apoptotic cell corpses are detected in the *n3246* and *n1993* alleles but not in *rp100* L1 animals. Data are expressed as mean ±SD and statistical significance was assessed using one-way ANOVA, with Tukey's multiple comparison test. ****<0.0001, n.s. not statistically significant comparing wild type and *ced-10* alleles (n = 30), over three independent scorings.(E) Brood size of *ced-10* hypomorphic alleles. *n3246* and *n1993* exhibit reduced brood size, whereas, *rp100* has a similar brood to wild type. Data are expressed as mean ±SD and statistical significance was assessed using one-way ANOVA, with Tukey's multiple comparison test. ***<0.0001, n.s. not statistically significant comparing wild type and *ced-10* alleles n = 30, each dot represents independent scoring replicates.(F) Summary of the effect of CED-10 hypomorphic mutations on PVQ axon outgrowth and guidance, apoptotic cell corpse engulfment and fecundity.

https://doi.org/10.1371/journal.pgen.1007670.g003

impact of these *ced-10* hypomorphic mutations (*rp100*, *n3246* and *n1993*) on PVQ development (S2A and S2B Fig). First, we found that all three alleles are recessive, such that one wild type copy of *ced-10* is able to coordinate PVQ axon outgrowth and guidance (S2A and S2B Fig). We then generated transheterozygote combinations between the alleles. We noticed that all transheterozygotes exhibited 30–40% PVQ developmental defects, which is approximately half the penetrance observed in *rp100* or *n3246* homozygotes (S2A Fig). This indicates that none of the mutated CED-10 proteins are able to fully compensate for each other. In contrast, both the *n3246* and *n1993* alleles can fully compensate the PVQ outgrowth defects of *rp100* animals (S2B Fig). The *n1993/rp100* transheterozygote exhibits a residual ~10% penetrant defect in PVQ axon outgrowth. This phenotype is not significantly different from wild type, however, and may suggest that a CED-10 protein with diminished membrane targeting cannot fully compensate for the defects caused by CED-10(G30E). Taken together, these data show that the G30E substitution in the *rp100* allele has a specific effect on PVQ axon outgrowth, not observed in other hypomorphic mutations in *ced-10*.

CED-10(G30E) does not disrupt canonical CED-10 functions

Thus far, we have shown that genetic lesions affecting specific domains, or residues, in the CED-10 protein can exhibit context-specific effects. We wanted to determine whether these differential phenotypic consequences are also observed for CED-10 function outside the nervous system. Therefore, we compared the effect of the *rp100*, *n3246* and *n1993* alleles in other well-characterized *ced-10* phenotypes—apoptotic corpse engulfment and fecundity (Fig 3D and 3E) [16, 36]. The number of persistent apoptotic cell corpses was counted in the heads of freshly hatched larval stage 1 (L1) animals harboring mutations in three *ced-10* alleles (Fig 3D). As previously reported, multiple persistent cell corpses were present in *n3246* and *n1993* mutant animals (Fig 3D) [36]. In stark contrast, we did not detect any persistent cell corpses in *rp100* mutant animals, as in wild type animals (Fig 3D). To ask whether *rp100* causes defects in apoptotic corpse engulfment at an earlier developmental stage, we performed a time-course analysis during embryogenesis (S3 Fig). We found that there was a statistically significant increase in the number of persistent cell corpses at the 1.5-fold and 2-fold stages of embryogenesis between *ced-10(rp100)* and wild type embryos; however, these corpses were cleared by the time of hatching (S3C Fig). We next asked whether we could enhance this partial delay in corpse engulfment in the *ced-10(rp100)* mutant by removing genes that are important for the two convergent pathways that control apoptotic corpse engulfment (S3D Fig). Double mutants of *ced-10(rp100)* and the adaptor protein CED-6/GULP [37], or the guanine nucleotide

exchange complex subunit CED-12/ELMO [38], had no significant effect on the number of persistent apoptotic corpses present at the L1 stage (S3D Fig). Taken together, the *ced-10 (rp100)* mutation has minimal, if any, effect on apoptotic corpse engulfment, which delineates it from the other known *ced-10* alleles.

We have shown that the molecular pathways dysregulated in *ced-10(rp100)* mutant animals do not adversely affect apoptotic corpse engulfment. In a reciprocal experiment, we asked whether signalling components through which CED-10 controls apoptotic cell recognition, engulfment and removal are required for PVQ axon outgrowth [39]. We examined the function of CED-1/LRP1/MEGF10, CED-2/CrkII and CED-5/Dock180, and found that these components of the apoptotic signaling pathway are dispensable for PVQ axon outgrowth (S3E Fig). We did find that *ced-5(tm1949)* mutant animals exhibit ~35% penetrant defects in PVQ guidance (S3F Fig), which suggests a function for CED-5 upstream of CED-10 in axonal development, as previously suggested [27]. These data show that the detrimental effect of the *ced-10 (rp100)* mutation on PVQ axon outgrowth is not likely due to defective interpretations of signals from the core apoptotic corpse engulfment machinery.

CED-10 is also important for coordinating how cells change shape and move during embryogenesis [40, 41]. As a result, reduction of CED-10 function normally results in embryonic lethality and reduced brood size [42]. We therefore counted the broods of *rp100*, *n3246* and *n1993* mutant animals (Fig 3E). As previously reported, the *n3246* and *n1993* alleles cause a marked reduction in brood, whereas, the *rp100* allele generates a similar brood size to wild type animals (Fig 3E). Taken together, these data show that mutations in CED-10 have context-specific effects during *C. elegans* development, potentially due to differential requirements of regulatory and/or effector interactions with specific regions of CED-10 and/or CED-10 activity (Fig 3F).

CED-10 domain mutations have neuron-specific effects during development

Multiple decisions during neuronal development require CED-10 function [16, 35, 43]. To understand the broader impact of the *ced-10(rp100)* mutation on neurodevelopment compared to the *n3246* and *n1993* mutations, we crossed all three alleles into fluorescent reporter strains to permit visualization of neuronal development at single-neuron resolution (S2 Table). We found that, in general, the membrane targeting-defective *n1993* allele had the weakest effect on neuronal development. However, the *n1993* allele did cause guidance defects in VNC neurons, left/right (L/R) choice of the VD motor neurons, and in the PLM and PVM neurons (S2 Table). In contrast, the two Switch region alleles, *rp100* and *n3246*, had stronger and comparable effects on neuronal guidance, with a few notable exceptions (S2 Table). In general, neurons that navigate the VNC are more strongly affected by *rp100* than *n3246*. For example, defects in PVP and HSN axon guidance, and AVG outgrowth exhibited higher penetrance in *rp100* than *n3246* (S2 Table). In addition, the *rp100* allele exhibits higher penetrant defects in DD and VD motor neuron commissure guidance (S2 Table). In contrast, PDE, AQR and mechanosensory neurons (ALM, AVM, PLM and PVM) development is more strongly affected by the *n3246* allele (S2 Table). Taken together, these data uncover the domain-specific roles of CED-10 in *C. elegans* neuronal outgrowth and guidance.

CED-10(G30E) causes defects in PVQ outgrowth through specific effector molecules

Rac GTPases interact with multiple regulatory and effector molecules to control a vast array of biological processes. The effect of the CED-10(G30E) mutation on axon outgrowth could be

due to a change in affinity with interacting molecules and/or altered activity or expression of its effector molecules. To determine the pathways through which defective CED-10(G30E) protein may cause PVQ outgrowth defects, we performed single and double mutant analysis with *ced-10(rp100)* and candidate genes that encode known Rac GTPase interactors or are known to regulate cytoskeletal remodelling at the growth cone (S1 Table).

We first focused our analysis on known Rac GTPase interactors. RIN-1 is a VPS9 domain protein that interacts with GTP-bound CED-10 and controls neuronal guidance downstream of Slit-Robo signalling [44]. We found that RIN-1 is not required for PVQ development and that the penetrance of *ced-10(rp100)* PVQ defects is not affected by the *rin-1(gk431)* mutation (S1 Table). Next, we examined the Lamellipodin homolog MIG-10, a major regulator of actin polymerisation to promote axon outgrowth [45, 46]. Surprisingly, *mig-10(ct41)* null mutant animals exhibit minimal PVQ axon outgrowth defects (2%), albeit with highly penetrant guidance defects (75%), and does not affect the PVQ outgrowth penetrance of *ced-10(rp100)* mutant animals (S1 Table). This indicates that MIG-10/Lamellipodin is not a crucial regulator of PVQ axon outgrowth. The *C. elegans* abLIM homolog UNC-115 is an actin modulatory protein that functions to control growth cone filopodia formation [47–49]. We found that UNC-115 is also dispensable for PVQ axon outgrowth and *unc-115(ky275)* null mutant animals exhibit a low penetrant axon guidance defect (S1 Table). The penetrance of PVQ axon guidance defects of *unc-115(ky275); ced-10(rp100)* animals is additive when compared to either single mutant suggesting that these factors regulate PVQ guidance in parallel (S1 Table).

Next, we analysed the function of the p21-activated kinases (PAKs), which are known downstream Rac GTPase effectors that are important for controlling cytoskeletal dynamics. Dimerized PAKs interact with GTP-bound Rac proteins, which relieves PAK self-inhibition and permit kinase domain activation [50]. We analysed PVQ development using mutant alleles of the *pak-1*, *pak-2* and *max-2* genes (S1 Table). We found that neither the *pak-2(ok332)* nor *max-2(ok1904)* mutants caused PVQ outgrowth defects. However, *max-2(ok1904)* animals do exhibit PVQ axon guidance defects, consistent with the finding that MAX-2 can regulate axon guidance independently of Rac proteins [51]. Furthermore, removing these PAK proteins had no effect on *ced-10(rp100)* PVQ axon outgrowth defects. In contrast, we found that two independent alleles of *pak-1* suppress the PVQ outgrowth defects of *ced-10(rp100)* mutant animals, without affecting the penetrance of PVQ guidance defects (S1 Table). One interpretation of these data is that PAK-1 acts in a parallel pathway to CED-10 in the PVQ neurons and that loss of PAK-1 affects outgrowth behavior such that the *ced-10(rp100)*-induced defects are suppressed. Alternatively, our observations could mean that CED-10(G30E) protein specifically alters PAK-1-regulated outgrowth.

Neurabin inhibits PVQ outgrowth

To identify additional molecular components that facilitate the *ced-10(rp100)* PVQ axon outgrowth defects, we performed a forward genetic suppressor screen (Fig 4A). Approximately 60% of *ced-10(rp100)* animals exhibit PVQ outgrowth defects when cultivated at 25°C (Fig 1C). Therefore, we mutagenized the *ced-10(rp100); oyIs14* strain with ethyl methanesulfonate and screened for reduced PVQ outgrowth defects in the progeny of 1000 F2 animals cultivated at 25°C. Of the four independent alleles that significantly suppress *ced-10(rp100)* PVQ outgrowth defects, we focus on *rp117*, a recessive allele that reduces *ced-10(rp100)* PVQ outgrowth defects at 20°C from ~35% to ~10% (Fig 4). Using bulk segregant mapping [52], we identified a premature ochre stop codon (TAT-TAA) in *nab-1*, which encodes the sole *C. elegans* ortholog of mammalian Neurabin (Fig 4B) [53, 54]. Using two, independent, *nab-1* deletion alleles, *gk164* and *ok943*, we confirmed that loss of *nab-1* supresses the *ced-10(rp100)* PVQ outgrowth
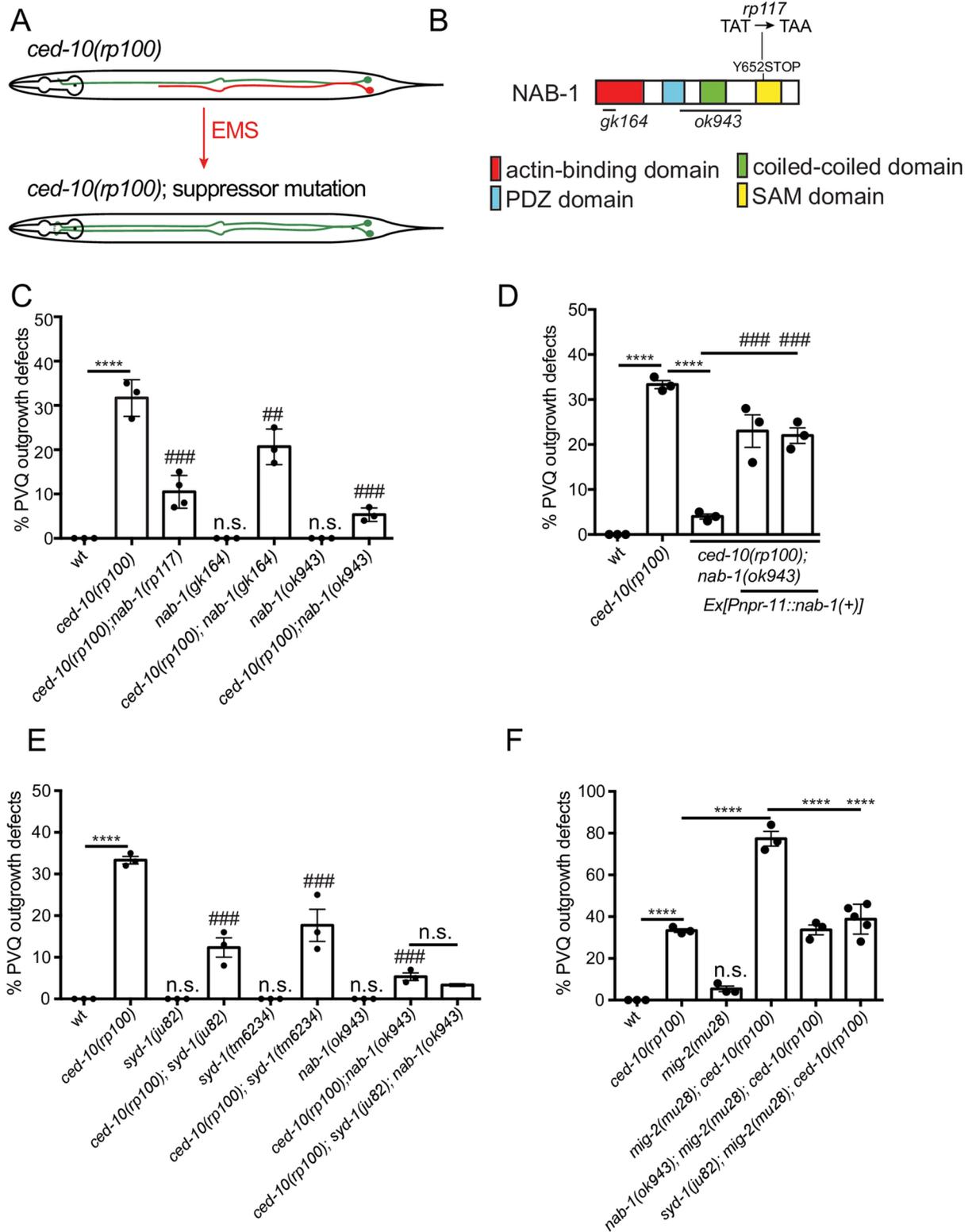
Fig 4. NAB-1 inhibits PVQ axon outgrowth. (A) Suppressor screen strategy (see main text). PVQL/R were marked by the *Psra-6::gfp* transgene. An outgrowth defect in the *ced-100(rp100)* strain is depicted by the red axon in the upper schematic. (B) Protein domain structure of *C. elegans* NAB-1. The allele obtained from the suppressor screen (*rp117*) and deletion strains (*gk164* and *ok943*) used in this study are indicated. (C) Loss-of-function alleles of *nab-1* (*rp117*, *gk164* and *ok943*) suppress the PVQ outgrowth defects of *ced-10(rp100)* animals. Data

are expressed as mean ±SD and statistical significance was assessed using one-way ANOVA, with Tukey's multiple comparison test. ****<0.0001, comparing wild type and *ced-10(rp100)* animals, ## = 0.0006 and ###<0.0001, comparing compound mutants to *ced-10(rp100)*. n. s. not statistically significant when compared to wild type. n = 90 per strain, each dot represents independent scoring replicates. (D) Transgenic expression of *nab-1* cDNA controlled by a PVQ-specific (*Pnpr-11*) promoter reverses the suppression of *ced-10(rp100)* PVQ outgrowth defects in *ced-10(rp100); nab-1(ok943)* animals. Data are expressed as mean ±SD and statistical significance was assessed using one-way ANOVA, with Tukey's multiple comparison test. ****<0.0001, comparing wild type and *ced-10(rp100)* animals or *ced-10(rp100)* and *ced-10(rp100); nab-1 (ok943)* animals; ###<0.0001 comparing the two transgenic rescue lines to *ced-10(rp100); nab-1(ok943)*. n = 90 per strain, each dot represents independent scoring replicates. (E) Loss-of-function alleles of *syd-1* (*ju82* and *tm6234*) suppress the PVQ outgrowth defects of *ced-10(rp100)* animals. The *ced-10(rp100); syd-1(ju82); nab-1(ok943)* triple mutant has similar PVQ outgrowth defects as the *ced-10(rp100); nab-1(ok943)* double mutant. Data are expressed as mean ±SD and statistical significance was assessed using one-way ANOVA, with Tukey's multiple comparison test. ****<0.0001, comparing wild type and *ced-10(rp100)* animals, ###<0.0001, comparing compound mutants to *ced-10(rp100)*. n.s. not statistically significant when compared to wild type or *ced-10(rp100); nab-1(ok943)* compared to *ced-10(rp100); syd-1(ju82); nab-1 (ok943)*. n = 90 per strain, each dot represents independent scoring replicates. (F) The highly penetrant PVQ outgrowth defects of *ced-10 (rp100); mig-2(mu28)* animals is suppressed by mutations in either *nab-1(ok943)* or *syd-1(ju82)*. Data are expressed as mean ±SD and statistical significance was assessed using one-way ANOVA, with Tukey's multiple comparison test. ****<0.0001, n.s. not statistically significant when compared to wild type. n = 90 per strain, each dot represents independent scoring replicates.

defects (Fig 4B and 4C). Interestingly, loss of *nab-1* does not suppress PVQ axon guidance defects (S4 Fig) suggesting a specific role for NAB-1 in outgrowth. In addition, we found *nab-1* is dispensable for correct PVQ development in a wild type background (S4 Fig). To ask whether NAB-1 functions cell-autonomously to inhibit PVQ axon outgrowth in the *ced-10 (rp100)* mutant background, we expressed *nab-1* cDNA using a PVQ specific promoter (Fig 4D). We found that PVQ-expressed *nab-1* cDNA reversed the suppression of PVQ axon outgrowth defects observed in the *ced-10(rp100); nab-1(ok943)* double mutant (Fig 4D). This confirms that NAB-1 functions cell-autonomously in the PVQ neurons to control axon outgrowth in animals with reduced CED-10 activity.

The functional domains of NAB-1 include an N-terminal actin-binding domain, a PDZ domain, a coiled-coil region and a C-terminal sterile alpha motif (SAM domain) with putative protein and RNA binding function [54–56]. Previous studies on NAB-1/Neurabin function have largely focussed on its role in synaptogenesis and synaptic function [53, 54, 57]. During *C. elegans* synaptogenesis, NAB-1 recruits the SYD-1 RhoGAP to filamentous actin [54]. SYD-1 itself has also been shown to interact with and repress MIG-2/RhoG to control HSN axon guidance [58]. We hypothesized that losing NAB-1, and potentially SYD-1 recruitment, would lead to Rac GTPase activation and subsequent suppression of the *ced-10(rp100)* axon outgrowth defects. To test this hypothesis, we generated compound mutants between *ced-10 (rp100)* and two, independent, *syd-1* alleles (*ju82* and *tm6234*). We found that both *syd-1* alleles suppress *ced-10(rp100)* PVQ outgrowth defects (Fig 4E). Further, we found that removing both *nab-1* and *syd-1* did not further suppress *ced-10(rp100)* PVQ outgrowth defects, suggesting that these genes act in the same pathway to regulate neuronal outgrowth (Fig 4E).

Our data suggest that NAB-1 and SYD-1 are required to suppress Rac GTPase activity during PVQ axon outgrowth. We have shown that CED-10 and MIG-2 act redundantly in PVQ axon outgrowth (S1 Table), and a previous study revealed that MIG-2 is negatively controlled by SYD-1 [58]. Therefore, we hypothesized that loss of NAB-1 or SYD-1 activates MIG-2 and thereby promotes PVQ axon outgrowth. To test this hypothesis, we examined the effect of losing NAB-1 or SYD-1 in the *ced-10(rp100); mig-2(mu28)* double mutant, which exhibits highly penetrant defects in PVQ axon outgrowth (Fig 4F and S1 Table). If NAB-1 and SYD-1 act through MIG-2, we would expect no suppression of PVQ axon outgrowth defects in *ced-10 (rp100); mig-2(mu28)* animals. However, we found that PVQ axon outgrowth defects of *ced-10 (rp100); mig-2(mu28)* animals are suppressed when *nab-1* or *syd-1* are absent (Fig 4F). As *mig-2(mu28)* is a null allele, these data suggest that NAB-1 and SYD-1 can regulate the activity of alternative GTPases, or may directly regulate CED-10 to control PVQ axon outgrowth.
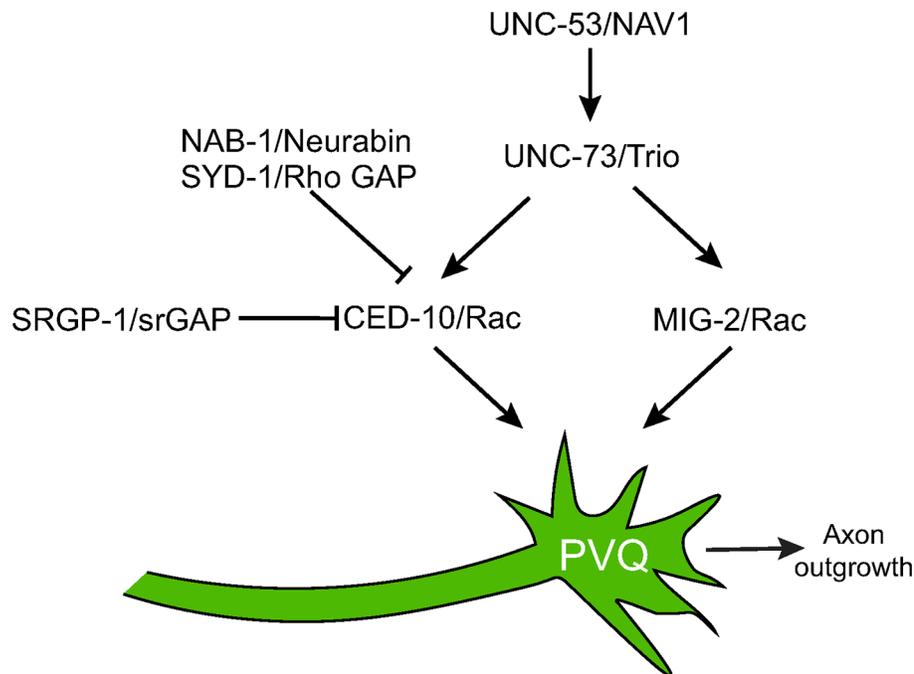
Fig 5. Control of CED-10 signaling in PVQ axon outgrowth. CED-10/Rac functions in parallel to MIG-2/Rac to control PVQ axon outgrowth. UNC-53/NAV1 and UNC-73/Trio act upstream of these Rac GTPases in a positive manner. Our study shows that mutations in upstream inhibitors of Rac activity (SRGP-1/Slit-Robo GAP and SYD-1/ Rho GAP) suppress PVQ axon outgrowth defects caused by a G30E mutation in the CED-10 protein. Loss of NAB-1/ Neurabin, a known interactor of SYD-1, also suppresses CED-10(G30E)-induced PVQ axon outgrowth defects, linking Neurabin proteins with the control of Rac GTPase activity.

https://doi.org/10.1371/journal.pgen.1007670.g005

Discussion

Axon outgrowth and guidance is coordinated by a plethora of extracellular signalling cues. Within the nascent axon, these cues are integrated through multiple, overlapping and non-overlapping, intracellular signaling cascades to ensure correct neuronal development. Rac GTPases are central to this process by acting as molecular switches to rapidly relay information through these signalling networks to enable appropriate axonal responses. In this study, we identified a single amino acid in the Switch 1 region of *C. elegans* CED-10/Rac1 that is crucial for regulating neuronal development (Fig 5). Focussing on the PVQ neurons, we found that a glycine to glutamic acid substitution at amino acid 30, CED-10(G30E), generates a CED-10 protein that causes severe axon outgrowth and guidance defects.

Our multiple lines of evidence show that the G30E substitution reduces CED-10 function. We have shown that *ced-10* null and *ced-10(rp100)* mutant animals exhibit similar PVQ axon outgrowth defects. In addition, PVQ axon outgrowth defects caused by *ced-10(rp100)* are fully recessive and are rescued by expressing wild type *ced-10* cDNA. We also demonstrate that animals harboring a known Rac1 hyperactive mutation (proline to serine substitution at position 29) in CED-10 did not exhibit PVQ axon outgrowth defects. Most importantly, using *in vitro* GTP activation assays we found that Rac1(G30E) is GTP activated ~50% less than wild type Rac1. The reduced affinity of CED-10(G30E) for GTP may result in diminished and/or atypical interactions between CED-10(G30E) and unknown effector molecule(s), thereby causing the PVQ axon outgrowth phenotype.

We found that the CED-10(G30E) mutant protein causes profound effects on PVQ outgrowth. However, unlike other CED-10 mutant proteins, CED-10(G30E) does not cause

defects in apoptotic corpse engulfment or fecundity. This suggests that defects in cell behaviour caused by the CED-10(G30E) protein specifically affects nervous system development. It could also suggest that the activity of CED-10(G30E) is not sufficiently reduced to impinge upon apoptotic corpse engulfment or generation of progeny. Focusing our analysis on the nervous system, we found that the neuronal guidance defects caused by CED-10(G30E) are similar to another mutation affecting the Switch 2 region, CED-10(G60R). However, we only found PVQ axon outgrowth defects in CED-10(G30E) animals. To our knowledge, this is the first report where different regions of Rac GTPases have been shown to differentially regulate axon outgrowth and guidance. Our data therefore suggest that PVQ outgrowth is especially sensitive to CED-10(G30E)-defective signaling and is an ideal model to delineate previously unknown functions for the Switch 1 region of Rac GTPases in regulating cell behaviour. Further analysis of the actin cytoskeletal architecture in the PVQ neurons during embryogenesis—the time of PVQ outgrowth, is unfortunately not presently feasible, as the tools to observe PVQ-specific reporter proteins during embryogenesis are unavailable.

We performed a genetic suppressor screen to identify the regulators controlling CED-10-directed PVQ axon outgrowth. This approach revealed that loss of NAB-1, the *C. elegans* Neurabin homolog, suppresses *ced-10(rp100)* PVQ axon outgrowth defects. In *C. elegans*, NAB-1 regulates synaptogenesis and synaptic function by binding to F-actin and recruiting the synaptic active zone proteins SYD-1 (RhoGAP) and SYD-2 (liprin-α) *[53, 54]*. In mammals, Neurabin I was originally shown to promote neurite formation in primary rat hippocampal neurons [59]. Further, in a neuroblastoma cell line, Neurabin I was shown to directly interact with Rac3, an interaction that is required for Rac3 induction of neuritogenesis [60]. Neurabin II/Spinophilin also controls dendritic spine formation, with reduction of Neurabin II causing an increase in spine density and altered filopodia formation [61]. Subsequent work showed that both increases and decreases in Neurabin I levels affect neurite outgrowth, suggesting that changes in Neurabin expression can disrupt the balance in downstream signaling pathways [62]. Supporting this, Neurabin is known to interact with multiple Rho GTPase modulators including GEFs (Lfc and Kalirin) and a GAP (SYD-1) [54, 63, 64]. Therefore, as a scaffolding protein NAB-1 may either promote or inhibit neurite outgrowth depending on the whether it coordinates binding of a Rho GTPase activator (GEF) or inhibitor (GAP). Evidence for this was revealed in studies of rat cortical neurons, where overexpression of Neurabin I reduced Rac1 activation, whereas knockdown activated Rac1 [62]. These data from mammalian systems support our findings that loss of NAB-1 promotes PVQ axon outgrowth in animals with diminished Rac GTPase activity. Further, our genetic data support previous biochemical studies where NAB-1 interacts with the Rho GAP SYD-1 to negatively regulate Rho GTPases [58].

Taken together, our work reveals that a conserved amino acid (glycine 30) in the CED-10/Rac1 protein is important for the activation status of this Rac GTPase and for correct axon outgrowth of the PVQ neurons in *C. elegans*. Rac GTPase activation status is central for regulating downstream effector pathways, and we found that the scaffolding protein NAB-1 and RhoGAP SYD-1 likely enhance CED-10 activity and therefore modify CED-10 output. Intriguingly, we found that although reduced NAB-1 and SYD-1 function promoted axon outgrowth, it did not restore PVQ axon guidance. This supports the hypothesis that there are intracellular mechanisms in growth cones that are specifically regulated by effector molecule binding to Rac GTPases, which differentially promote/inhibit axon outgrowth and guidance. We propose that identifying the precise effector molecules and pathways controlled by CED-10 under different levels of activation will uncover novel insights into how correct axon outgrowth and guidance is achieved.

Materials and methods

C. elegans strains and genetics

All *C. elegans* strains were maintained at 20˚C on NGM plates seeded with *Escherichia coli* OP50 bacteria, unless otherwise stated [65]. Strains were generated using standard genetic procedures and are listed in S3 and S4 Tables. All strains were backcrossed to N2 at least three times before scoring or generating compound mutants. Genotypes were confirmed using PCR genotyping or Sanger sequencing with primers listed in S5 Table.

Neuroanatomical observation and scoring

Neurons were scored, blinded to phenotype, in L4/young adult stages, unless otherwise stated. Scoring criteria for each neuron is detailed in S2 Table. The following transgenes were used to enable visualization of specific neurons. PVQs: *oyIs14*, *hdIs26*, *rpEx1640*; Mechanosensory neurons: (ALMs, AVM, PVM and PLMs) *zdIs5;* HSNs: *rpEx6;* PDEs: *lqIs2;* PVPs: *hdIs26;* AVGs: *otIs182;* D-type motor neurons: *oxIs12;* AQR: *rpIs8.* All neuronal scoring was repeated in triplicates on independent days, n = 75, except for *oxIs12* scoring, n = 35.

Genetic mapping of *ced-10(rp100)*

We initially observed PVQ axon outgrowth and guidance defects in the following strain—*nDf67(mir-51 mir-53* deletion); *oyIs14* [66]. After ten backcrosses with N2 males the PVQ outgrowth defects disappeared. We re-examined the ninth backcrossed strain, performed a backcross and randomly selected 50 F2 progeny. We screened the F3 progeny and found 14 plates that exhibited the PVQ outgrowth phenotype. Two of those where heterozygote for the *nDf67* deletion, from which we singled animals and genotyped for loss of the *nDf67* deletion. These animals still exhibited the PVQ outgrowth phenotype. We named the mutant allele *rp100* and used the one-step whole-genome sequencing and SNP mapping strategy to map the genetic lesion [24]. Males of the Hawaiian strain CB4856 were crossed with *rp100; oyIs14* hermaphrodites. Ten F1 progeny carrying the *oyIs14* transgene were picked to individual plates and allowed to self-fertilize. F2 progeny carrying the *oyIs14* transgene were picked to 250 individual plates and allowed to self-fertilize. Approximately 20 F3 progeny from each of the 250 F2 plates were scored for PVQ axon outgrowth defects. 47 plates were homozygous for the phenotype causing mutation, based on the presence of PVQ outgrowth defects. Progeny of these animals were pooled and DNA was isolated. Pooled genomic DNA was sequenced using Ilumina sequencing and the resultant sequencing data was analyzed using the Galaxy platform. Our mapping identified a single lesion (GGA-GAA) at base-pair position 89 within exon 1 of the *ced-10* gene, which was independently confirmed by Sanger sequencing.

Clonal EMS mutagenesis screen

Random mutations in *ced-10(rp100); oyIs14* animals were induced with ethyl methanesulfonate (EMS) following the modified version of a previously described protocol [65]. Since incubation at 25˚C increases the penetrance of PVQ axon outgrowth defects caused by *ced-10 (rp100)*, screening for suppressor mutations was conducted at 25˚C. The germlines of *ced-10 (rp100); oyIs14* animals (L4 stage) were mutagenised using 50mM EMS (Sigma) in M9 buffer (22 mM KH_2PO_4, 42 mM Na_2HPO_4, 86 mM NaCl) for 4 hours (room temperature), after which they were transferred to standard OP50 NGM plates for 72 hours (20˚C). F1s were allowed to self-fertilise on individual plates (20˚C). Four F2s (L4 stage) were randomly picked from each F1 and separated into individual plates for incubation at 25˚C. F3 populations with

PVQ outgrowth defects lower than 20% (n = 50) were selected and retested in subsequent generations for heritability of suppression.

Identification of *nab-1* as a suppressor of *ced-10(rp100)*

Suppressor gene identification was carried out using whole genome sequencing and bulk-segregant mapping [52]. Candidate lines carrying suppressor mutations were backcrossed with *ced-10(rp100); oyIs14* and 200 recombinant F2s from each cross were separated into individual plates for incubation at 25°C. Recombinant F2s homozygous for the suppressor mutation were identified by scoring for suppression of PVQ outgrowth defects of F3 offspring. 40 F2 plates exhibited the suppressor phenotype and worms were washed off with M9 buffer and pooled for DNA extraction with Gentra Puregene kit (Qiagen). Paired-end whole genome sequencing (WGS) with Illumina NextSeq500 was performed and the causative genetic lesion identified using Mutation Identification in Model Organism Genomes (MiMoDd) (version 0.1.7.3).

C. elegans plasmid generation

Plasmid inserts were confirmed using Sanger sequencing prior to use.

RJP273 *sra-6^{prom}::ced-10cDNAb*

ced-10 cDNA isoform b was amplified from an oligodT amplified cDNA library using the oligos 5'-ttggctagcgtcgacggtacatgcaagcgatcaaatgtg-3' and 5'-agatatcaataccatggtacttagagcaccgta-cactt-3' and ligated into a *sra-6^{prom}* plasmid with a pPD49.26 backbone using *KpnI*.

RJP272 *rgef-1^{prom}::ced-10cDNAb*

ced-10 cDNAb from RJP273 was ligated downstream of a *rgef-1^{prom}* in a pPD49.26 backbone using *NheI-SpeI*.

RJP296 *sra-6^{prom}::GFP*

Sequence encoding GFP was ligated into a *sra-6^{prom}* plasmid with a pPD49.26 backbone using *NheI-SpeI*.

RJP297 *sra-6^{prom}::mCherry*

Sequence encoding mCherry protein was ligated into a *sra-6^{prom}* plasmid with a pPD49.26 backbone using *NheI-SpeI*.

RJP370 *npr-11^{prom}::nab-1*

nab-1 cDNA was amplified from an oligodT amplified cDNA library using the oligos 5'-gctagcatgacaacggcttccgagc -3' and 5'- ggtacctcacatgggaattgtgtgtgc-3' and ligated into a *npr-11^{prom}* plasmid with a pPD49.26 backbone using *NheI-KpnI*.

Fluorescence microscopy

Animals were mounted on 5% agarose pads and immobilized using 50mM NaN$_3$. Examination and imaging of neurons was performed using an automated fluorescence microscope (Zeiss, AXIO Imager M2) and ZEN software (version 3.1).

Microinjections and transgenic animals

Transgenic animals were generated as previously described [67]. Rescue plasmids were injected directly into *ced-10(rp100); oyIs14*. The WRM0639dH09 fosmid spanning the entire *ced-10* locus was injected at 1ng/µl. For pan-neuronal rescue, RJP272 (*rgef-1^{prom}::ced-10cDNAb*) was injected at 10ng/µl. For cell-autonomous rescue, RJP273 (*sra-6^{prom}::ced-10cDNAb*) was injected at 50ng/µl and RJP370 *npr-11^{prom}::nab-1* at 10ng/µl. RJP370 (*npr-11^{prom}::nab-1*) was injected *into nab-1(ok943); ced-10(rp100); oyIs14* animals at 20ng/µl. *myo-2^{prom}::mCherry* was injected at 5ng/µl as a co-injection marker in all transgenic animals.

Mosaic analysis

For mosaic analysis, transgenic animals were generated by injecting RJP272 (*rgef-1^{prom}::ced-10cDNAb*) at 10ng/μl, RJP297 (*sra-6^{prom}::mCherry*) at 10ng/μl and *myo-2^{prom}::mCherry* at 5ng/μl into the *ced-10(rp100); oyIs14* strain. A transgenic line was selected that exhibited rescue of the PVQ axon outgrowth and guidance defects. Transgenic animals from this line were then scored for phenotypic rescue of the PVQ defects in the presence and absence of the rescuing extrachromosomal array in the PVQ neurons by detection of *mCherry* fluorescence.

Brood size

For each replicate, 10 individual mid-L4 larvae were placed on separate plates. Every 24 hrs, each worm was moved to a new plate and the previous plate was left for 24 hrs prior to scoring to allow enough time for all the laid eggs to hatch. The experiment was conducted in 3 replicates on independent days.

Scoring of apoptotic corpses

Mixed culture plates were washed thoroughly five times with M9 to remove all worms, leaving eggs behind. After 20 mins, freshly hatched L1 larvae were mounted on agarose and immediately scored by DIC optics for persistent cell corpses in the head (anterior to the posterior bulb of the pharynx).

Bacterial expression plasmid generation

pGEX-4T-1-TEV-Rac1$_{1-177}$ was obtained from Christina Lucato [68]. Point mutations in the Rac1 plasmids were generated using the Q5 site-directed mutagenesis kit (New England Biolabs) with the following oligonucleotides: pGEX-4T-1-TEV-Rac1(G30E): 5'-gcatttcctgaagaatatatccc-3', 5'-attggttgtgtaactgatcag-3'and pGEX-4T-1-TEV-Rac1(P29S):5'-caatgcattttctggagaatatatc-3',5'-gttgtgtaactgatcagtag-3'.

Protein purification of wild type and mutant Rac1 (residues 1–177)

pGEX-4T-1-TEV-Rac1 wild type and mutant plasmids were transformed into *Escherichia coli* BL21(DE3) CodonPlus cells and GST-Rac1 protein expression was induced by IPTG at 18˚C overnight. Cells were pelleted and resuspended in lysis buffer (20 mM Tris, pH 8.0, 500 mM NaCl, 2 mM DTT, and 2 mM EDTA). Cells were lysed by sonication and cell debris was cleared by centrifugation. Soluble lysate was filtered at 0.8 μm. GST-Affinity purification was carried out with glutathione-Sepharose 4B resin (GE Healthcare) at 4˚C for 90 min. The GST tag was cleaved with overnight incubation with TEV protease. Rac1 was eluted and further purified with size-exclusion chromatography on a HiLoad Superdex 75 16/60 column (GE Healthcare), equilibrated in SEC buffer (20 mM Tris, pH 8.0, 150 mM NaCl and 2 mM DTT).

in vitro Rac1 activation assay

Purified wild type and mutant Rac1 proteins (500 μM) in SEC buffer was preloaded with 10 mM GDP and 5 mM EDTA, for 1 hour at room temperature. The reaction was terminated by adding 10 mM MgCl$_2$ (final volume). EDTA and excess GDP is removed from GDP-loaded Rac1 with PD-10 desalting columns and equilibrated with 20 mM Tris, pH 8.0, 150 mM NaCl, 10 mM MgCl$_2$, 2mM DTT. 30 μM Rac1-GDP was incubated with 500 μM GTPγS with or without 15 mM EDTA for 1 hour at room temperature and the reaction was terminated by adding 20 mM MgCl$_2$ (final volume). 5 μg Rac1-nucleotide complexes were allowed to bind with 5 μg PAK-PDB beads (Cytoskeleton) in 500 μl of pulldown buffer (25mM Tris-HCl, pH 8.0, 40mM

NaCl, 30mM MgCl$_2$, 1 mM DTT, 1% (v/v) Igepal CA-630) for 1 hour at 4˚C. Beads were washed three times with cold pulldown buffer. Active Rac1 bound to PAK beads were eluted in Lithium Dodecyl Sulfate loading buffer and subjected to SDS-PAGE. Eluted Rac1 protein was detected by western blotting and anti-Rac1 mouse monoclonal antibody (Cytoskeleton). Western quantification was carried out with ImageJ with intensities normalised to loading controls. Method adapted from [26].

Statistical analysis

Statistical analysis was carried out using Graphpad Prism 7 using one-way ANOVA with Tukey's Multiple Comparison Test or t test, where applicable. Values are expressed as mean ±S.D. Values <0.05 were considered statistical significant.

Supporting information

S1 Fig. Related to Fig 1. *ced-10(rp100)* rescue and mosaic analysis.
(A) Alignment of the amino acid sequences of *Homo sapiens* Rac1 (HsRac1) and *C. elegans* CED-10 (CeCED-10). The *ced-10* point mutants used in this study are marked with an asterisk: *rp100* (G30E - Switch 1 region), *n3246* (G60R - Switch 2 region) and *n1993* (V190G - membrane targeting region).
(B) Quantification of pan-neuronal and PVQ-specific transgenic rescue of total PVQ defects of *ced-10(rp100)* animals with *ced-10* cDNA (*ced-10(+)*). Data are expressed as mean ±SD and statistical significance was assessed using one-way ANOVA, with Tukey's multiple comparison test. ****<0.0001, comparing wild type and *rp100* animals; #<0.0001 and +<0.006 and comparing the three transgenic rescue lines to *ced-10(rp100)*. n.s. not statistically significant from *rp100* animals. n = 90 per strain, each dot represents independent scoring replicates.
(C) An unstable transgenic array containing *Prgef-1*::*ced-10(+)*, *Psra-6*::*mCherry* and *Pmyo-2*::*mCherry* plasmids was expressed in *ced-10(rp100); oyIs14* animals. PVQ outgrowth and guidance was scored in animals in which the array was absent (*Psra-6*::*mCherry*, *Pmyo-2*::*mCherry* negative), present in the PVQs (*Psra-6*::*mCherry*, *Pmyo-2*::*mCherry* positive) or missing from the PVQs (*Psra-6*::*mCherry* negative, *Pmyo-2*::*mCherry* positive). Number of animals scored is shown in parentheses.
(PDF)

S2 Fig. Related to Fig 2. genetic analysis of *ced-10* alleles.
(A) Quantification of total PVQ defects (outgrowth and guidance) in wild type, *ced-10* mutant homozygotes, heterozygotes and transheterozygotes. Data are expressed as mean ±SD and statistical significance was assessed using one-way ANOVA, with Tukey's multiple comparison test. ****<0.0001, n.s. not significantly different to wild type. n = 90 per strain, each dot represents independent scoring replicates.
(B) Quantification of PVQ outgrowth defects in wild type, *ced-10* mutant homozygotes, heterozygotes and transheterozygotes. Data are expressed as mean ±SD and statistical significance was assessed using one-way ANOVA, with Tukey's multiple comparison test. ****<0.0001, n.s. not significantly different to wild type. n = 90 per strain, each dot represents independent scoring replicates.
(C) Quantification of PVQ outgrowth defects in wild type L1 larvae and *ced-10(tm597)* L1 escapers. Data are expressed as mean ±SD and statistical significance was assessed using t test. n = 9 per strain, each dot represents independent scoring replicates.
(PDF)

S3 Fig. Related to Fig 3. apoptotic pathway function.

(A) Images of the heads of freshly hatched L1 animals. Persistent apoptotic cell corpses are marked with white arrows.

(B) Quantification of apoptotic corpse engulfment in *ced-10* mutant animals. The number of persistent cell corpses was counted at the bean stage of embryogenesis. Data are expressed as mean ±SD and statistical significance was assessed using one-way ANOVA, with Tukey's multiple comparison test. ****<0.0001, n.s., not statistically significant from wild type. n = 21, from three independent scorings.

(C) Quantification of apoptotic corpse engulfment in wild type and *ced-10(rp100)* mutant animals. Data are expressed as mean ±SD and statistical significance was assessed using one-way ANOVA, with Tukey's multiple comparison test. ****<0.0001, *<0.01, n.s., not statistically significant from wild type. n = 15, from three independent scorings.

(D) Quantification of persistent cell corpses present in the head of freshly hatched *ced-10 (rp100)* L1 larvae combined with mutations in CED-6/GULP and CED-12/ELMO. Data are expressed as mean ±SD and statistical significance was assessed using one-way ANOVA, with Tukey's multiple comparison test. n.s. not statistically significant comparing *ced-6* and *ced-12* single mutants combined with *ced-10(rp100)*. n = 17, from three independent scorings.

(E) Quantification of PVQ outgrowth defects in wild type and mutants of apoptotic pathway genes. Data are expressed as mean ±SD and statistical significance was assessed using one-way ANOVA, with Tukey's multiple comparison test. ****<0.0001, n.s. not significantly different to wild type. n = 75 per strain, each dot represents independent scoring replicates.

(F) Quantification of total PVQ defects (outgrowth and guidance) in wild type and mutations in apoptotic pathway genes. Data are expressed as mean ±SD and statistical significance was assessed using one-way ANOVA, with Tukey's multiple comparison test. ****<0.0001, n.s. not significantly different to wild type. n = 75 per strain, each dot represents independent scoring replicates.

(PDF)

S4 Fig. Related to Fig 4. genetic analysis of NAB-1 function in PVQ development. Quantification of total PVQ defects (outgrowth and guidance) in wild type, *ced-10(rp100)* and compound mutants between *ced-10(rp100)* and *nab-1* alleles (*rp117*, *gk164* and *ok943*). Data are expressed as mean ±SD and statistical significance was assessed using one-way ANOVA, with Tukey's multiple comparison test. ****<0.0001, comparing wild type and *rp100* animals, n.s. not statistically significant when compared to either wild type (for single mutants) or *ced-10 (rp100)* for compound mutants. n = 90 per strain, each dot represents independent scoring replicates.

(PDF)

S1 Table. Genetic analysis of candidate CED-10/Rac1 regulatory and effector molecules.
(PDF)

S2 Table. Neuroanatomical analysis of *ced-10* mutant function.
(PDF)

S3 Table. List of strains used in this study.
(PDF)

S4 Table. List of mutant alleles used in this study.
(PDF)

S5 Table. List of genotyping primers used in this study.
(PDF)

Acknowledgments

Author Contributions

References

1. White JG, Southgate E, Thomson JN, Brenner S. The structure of the ventral nerve cord of Caenorhabditis elegans. Philos Trans R Soc Lond B Biol Sci. 1976; 275(938):327–48. PMID: 8806

2. Pocock R, Hobert O. Oxygen levels affect axon guidance and neuronal migration in Caenorhabditis elegans. Nat Neurosci. 2008; 11(8):894–900. Epub 2008/07/01. nn.2152 [pii] https://doi.org/10.1038/nn.2152 PMID: 18587389.

3. Bülow HE, Boulin T, Hobert O. Differential functions of the C. elegans FGF receptor in axon outgrowth and maintenance of axon position. Neuron. 2004; 42(3):367–74. PMID: 15134634.

4. Boulin T, Pocock R, Hobert O. A novel Eph receptor-interacting IgSF protein provides C. elegans moto-neurons with midline guidepost function. Curr Biol. 2006; 16(19):1871–83. https://doi.org/10.1016/j.cub.2006.08.056 PMID: 17027485.

5. Steimel A, Wong L, Najarro EH, Ackley BD, Garriga G, Hutter H. The Flamingo ortholog FMI-1 controls pioneer-dependent navigation of follower axons in C. elegans. Development. 2010; 137(21):3663–73. https://doi.org/10.1242/dev.054320 PMID: 20876647; PubMed Central PMCID: PMCPMC2959053.

6. Hutter H. Formation of longitudinal axon pathways in Caenorhabditis elegans. Semin Cell Dev Biol. 2017. https://doi.org/10.1016/j.semcdb.2017.11.015 PMID: 29141179.

7. Torpe N, Pocock R. Regulation of axonal midline guidance by prolyl 4-hydroxylation in Caenorhabditis elegans. J Neurosci. 2014; 34(49):16348–57. https://doi.org/10.1523/JNEUROSCI.1322-14.2014 PMID: 25471573; PubMed Central PMCID: PMCPMC4252547.

8. Aurelio O, Hall DH, Hobert O. Immunoglobulin-domain proteins required for maintenance of ventral nerve cord organization. Science. 2002; 295(5555):686–90. https://doi.org/10.1126/science.1066642 PMID: 11809975

9. Zallen JA, Yi BA, Bargmann CI. The conserved immunoglobulin superfamily member SAX-3/Robo directs multiple aspects of axon guidance in C. elegans. Cell. 1998; 92(2):217–27. PMID: 9458046

10. Wightman B, Baran R, Garriga G. Genes that guide growth cones along the C. elegans ventral nerve cord. Development. 1997; 124(13):2571–80. PMID: 9216999

11. Tessier-Lavigne M, Goodman CS. The molecular biology of axon guidance. Science. 1996; 274 (5290):1123–33. PMID: 8895455

12. Dent EW, Gupton SL, Gertler FB. The growth cone cytoskeleton in axon outgrowth and guidance. Cold Spring Harb Perspect Biol. 2011; 3(3). https://doi.org/10.1101/cshperspect.a001800 PMID: 21106647; PubMed Central PMCID: PMCPMC3039926.

13. Hall A. Rho GTPases and the actin cytoskeleton. Science. 1998; 279(5350):509–14. PMID: 9438836.

14. Luo L. Rho GTPases in neuronal morphogenesis. Nat Rev Neurosci. 2000; 1(3):173–80. https://doi.org/ 10.1038/35044547 PMID: 11257905.

15. Govek EE, Newey SE, Van Aelst L. The role of the Rho GTPases in neuronal development. Genes Dev. 2005; 19(1):1–49. https://doi.org/10.1101/gad.1256405 PMID: 15630019.

16. Lundquist EA, Reddien PW, Hartwieg E, Horvitz HR, Bargmann CI. Three C. elegans Rac proteins and several alternative Rac regulators control axon guidance, cell migration and apoptotic cell phagocytosis. Development. 2001; 128(22):4475–88. PMID: 11714673

17. Kuhn TB, Brown MD, Bamburg JR. Rac1-dependent actin filament organization in growth cones is necessary for beta1-integrin-mediated advance but not for growth on poly-D-lysine. J Neurobiol. 1998; 37 (4):524–40. PMID: 9858256.

18. Luo L, Liao YJ, Jan LY, Jan YN. Distinct morphogenetic functions of similar small GTPases: Drosophila Drac1 is involved in axonal outgrowth and myoblast fusion. Genes Dev. 1994; 8(15):1787–802. PMID: 7958857.

19. Kinsella BT, Erdman RA, Maltese WA. Carboxyl-terminal isoprenylation of ras-related GTP-binding proteins encoded by rac1, rac2, and ralA. J Biol Chem. 1991; 266(15):9786–94. PMID: 1903399.

20. Etienne-Manneville S, Hall A. Rho GTPases in cell biology. Nature. 2002; 420(6916):629–35. https:// doi.org/10.1038/nature01148 PMID: 12478284.

21. Vetter IR, Wittinghofer A. The guanine nucleotide-binding switch in three dimensions. Science. 2001; 294(5545):1299–304. https://doi.org/10.1126/science.1062023 PMID: 11701921.

22. Bos JL, Rehmann H, Wittinghofer A. GEFs and GAPs: critical elements in the control of small G proteins. Cell. 2007; 129(5):865–77. https://doi.org/10.1016/j.cell.2007.05.018 PMID: 17540168.

23. Rossman KL, Der CJ, Sondek J. GEF means go: turning on RHO GTPases with guanine nucleotide-exchange factors. Nat Rev Mol Cell Biol. 2005; 6(2):167–80. https://doi.org/10.1038/nrm1587 PMID: 15688002.

24. Doitsidou M, Poole RJ, Sarin S, Bigelow H, Hobert O. C. elegans mutant identification with a one-step whole-genome-sequencing and SNP mapping strategy. PLoS One. 2010; 5(11):e15435. https://doi. org/10.1371/journal.pone.0015435 PMID: 21079745; PubMed Central PMCID: PMCPMC2975709.

25. Worthylake DK, Rossman KL, Sondek J. Crystal structure of Rac1 in complex with the guanine nucleotide exchange region of Tiam1. Nature. 2000; 408(6813):682–8. https://doi.org/10.1038/35047014 PMID: 11130063.

26. Davis MJ, Ha BH, Holman EC, Halaban R, Schlessinger J, Boggon TJ. RAC1P29S is a spontaneously activating cancer-associated GTPase. Proc Natl Acad Sci U S A. 2013; 110(3):912–7. https://doi.org/ 10.1073/pnas.1220895110 PMID: 23284172; PubMed Central PMCID: PMCPMC3549122.

27. Wu YC, Cheng TW, Lee MC, Weng NY. Distinct rac activation pathways control Caenorhabditis elegans cell migration and axon outgrowth. Dev Biol. 2002; 250(1):145–55. PMID: 12297102.

28. Manser E, Leung T, Salihuddin H, Zhao ZS, Lim L. A brain serine/threonine protein kinase activated by Cdc42 and Rac1. Nature. 1994; 367(6458):40–6. https://doi.org/10.1038/367040a0 PMID: 8107774.

29. Dickinson DJ, Ward JD, Reiner DJ, Goldstein B. Engineering the Caenorhabditis elegans genome using Cas9-triggered homologous recombination. Nat Methods. 2013; 10(10):1028–34. https://doi.org/ 10.1038/nmeth.2641 PMID: 23995389; PubMed Central PMCID: PMCPMC3905680.

30. Zheng C, Diaz-Cuadros M, Chalfie M. GEFs and Rac GTPases control directional specificity of neurite extension along the anterior-posterior axis. Proc Natl Acad Sci U S A. 2016; 113(25):6973–8. https:// doi.org/10.1073/pnas.1607179113 PMID: 27274054; PubMed Central PMCID: PMCPMC4922148.

31. van Haren J, Boudeau J, Schmidt S, Basu S, Liu Z, Lammers D, et al. Dynamic microtubules catalyze formation of navigator-TRIO complexes to regulate neurite extension. Curr Biol. 2014; 24(15):1778–85. https://doi.org/10.1016/j.cub.2014.06.037 PMID: 25065758.

32. deBakker CD, Haney LB, Kinchen JM, Grimsley C, Lu M, Klingele D, et al. Phagocytosis of apoptotic cells is regulated by a UNC-73/TRIO-MIG-2/RhoG signaling module and armadillo repeats of CED-12/ ELMO. Curr Biol. 2004; 14(24):2208–16. https://doi.org/10.1016/j.cub.2004.12.029 PMID: 15620647.

33. Neukomm LJ, Frei AP, Cabello J, Kinchen JM, Zaidel-Bar R, Ma Z, et al. Loss of the RhoGAP SRGP-1 promotes the clearance of dead and injured cells in Caenorhabditis elegans. Nat Cell Biol. 2011; 13 (1):79–86. https://doi.org/10.1038/ncb2138 PMID: 21170032; PubMed Central PMCID: PMCPMC3808961.

34. Ellis RE, Jacobson DM, Horvitz HR. Genes required for the engulfment of cell corpses during programmed cell death in Caenorhabditis elegans. Genetics. 1991; 129(1):79–94. PMID: 1936965; PubMed Central PMCID: PMCPMC1204584.

35. Hedgecock EM, Sulston JE, Thomson JN. Mutations affecting programmed cell deaths in the nematode Caenorhabditis elegans. Science. 1983; 220(4603):1277–9. Epub 1983/06/17. PMID: 6857247.

36. Reddien PW, Horvitz HR. CED-2/CrkII and CED-10/Rac control phagocytosis and cell migration in Caenorhabditis elegans. Nat Cell Biol. 2000; 2(3):131–6. https://doi.org/10.1038/35004000 PMID: 10707082.

37. Liu QA, Hengartner MO. Candidate adaptor protein CED-6 promotes the engulfment of apoptotic cells in C. elegans. Cell. 1998; 93(6):961–72. PMID: 9635426.

38. Zhou Z, Caron E, Hartwieg E, Hall A, Horvitz HR. The C. elegans PH domain protein CED-12 regulates cytoskeletal reorganization via a Rho/Rac GTPase signaling pathway. Dev Cell. 2001; 1(4):477–89. PMID: 11703939.

39. Reddien PW, Horvitz HR. The engulfment process of programmed cell death in caenorhabditis elegans. Annu Rev Cell Dev Biol. 2004; 20:193–221. https://doi.org/10.1146/annurev.cellbio.20.022003.114619 PMID: 15473839.

40. Soto MC, Qadota H, Kasuya K, Inoue M, Tsuboi D, Mello CC, et al. The GEX-2 and GEX-3 proteins are required for tissue morphogenesis and cell migrations in C. elegans. Genes Dev. 2002; 16(5):620–32. https://doi.org/10.1101/gad.955702 PMID: 11877381; PubMed Central PMCID: PMCPMC155352.

41. Walck-Shannon E, Reiner D, Hardin J. Polarized Rac-dependent protrusions drive epithelial intercalation in the embryonic epidermis of C. elegans. Development. 2015; 142(20):3549–60. https://doi.org/10.1242/dev.127597 PubMed Central PMCID: PMCPMC4631769. PMID: 26395474

42. Kinchen JM, Cabello J, Klingele D, Wong K, Feichtinger R, Schnabel H, et al. Two pathways converge at CED-10 to mediate actin rearrangement and corpse removal in C. elegans. Nature. 2005; 434 (7029):93–9. https://doi.org/10.1038/nature03263 PMID: 15744306.

43. Patel FB, Bernadskaya YY, Chen E, Jobanputra A, Pooladi Z, Freeman KL, et al. The WAVE/SCAR complex promotes polarized cell movements and actin enrichment in epithelia during C. elegans embryogenesis. Dev Biol. 2008; 324(2):297–309. https://doi.org/10.1016/j.ydbio.2008.09.023 PMID: 18938151; PubMed Central PMCID: PMCPMC2629559.

44. Doi M, Minematsu H, Kubota Y, Nishiwaki K, Miyamoto M. The novel Rac effector RIN-1 regulates neuronal cell migration and axon pathfinding in C. elegans. Development. 2013; 140(16):3435–44. https://doi.org/10.1242/dev.089722 PMID: 23900541; PubMed Central PMCID: PMCPMC4074257.

45. Quinn CC, Pfeil DS, Chen E, Stovall EL, Harden MV, Gavin MK, et al. UNC-6/netrin and SLT-1/slit guidance cues orient axon outgrowth mediated by MIG-10/RIAM/lamellipodin. Curr Biol. 2006; 16(9):845–53. https://doi.org/10.1016/j.cub.2006.03.025 PMID: 16563765.

46. Quinn CC, Pfeil DS, Wadsworth WG. CED-10/Rac1 mediates axon guidance by regulating the asymmetric distribution of MIG-10/lamellipodin. Curr Biol. 2008; 18(11):808–13. https://doi.org/10.1016/j.cub.2008.04.050 PMID: 18499456; PubMed Central PMCID: PMCPMC2702229.

47. Gitai Z, Yu TW, Lundquist EA, Tessier-Lavigne M, Bargmann CI. The netrin receptor UNC-40/DCC stimulates axon attraction and outgrowth through enabled and, in parallel, Rac and UNC-115/AbLIM. Neuron. 2003; 37(1):53–65. PMID: 12526772.

48. Lundquist EA, Herman RK, Shaw JE, Bargmann CI. UNC-115, a conserved protein with predicted LIM and actin-binding domains, mediates axon guidance in C. elegans. Neuron. 1998; 21(2):385–92. Epub 1998/09/05. S0896-6273(00)80547-4 [pii]. PMID: 9728919.

49. Struckhoff EC, Lundquist EA. The actin-binding protein UNC-115 is an effector of Rac signaling during axon pathfinding in C. elegans. Development. 2003; 130(4):693–704. PMID: 12506000.

50. Bokoch GM. Biology of the p21-activated kinases. Annu Rev Biochem. 2003; 72:743–81. https://doi.org/10.1146/annurev.biochem.72.121801.161742 PMID: 12676796.

51. Lucanic M, Kiley M, Ashcroft N, L'Etoile N, Cheng HJ. The Caenorhabditis elegans P21-activated kinases are differentially required for UNC-6/netrin-mediated commissural motor axon guidance. Development. 2006; 133(22):4549–59. https://doi.org/10.1242/dev.02648 PMID: 17050621.

52. Minevich G, Park DS, Blankenberg D, Poole RJ, Hobert O. CloudMap: a cloud-based pipeline for analysis of mutant genome sequences. Genetics. 2012; 192(4):1249–69. https://doi.org/10.1534/genetics.112.144204 PMID: 23051646; PubMed Central PMCID: PMCPMC3512137.

53. Hung W, Hwang C, Po MD, Zhen M. Neuronal polarity is regulated by a direct interaction between a scaffolding protein, Neurabin, and a presynaptic SAD-1 kinase in Caenorhabditis elegans. Development. 2007; 134(2):237–49. Epub 2006/12/08. dev.02725 [pii] https://doi.org/10.1242/dev.02725 PMID: 17151015.

54. Chia PH, Patel MR, Shen K. NAB-1 instructs synapse assembly by linking adhesion molecules and F-actin to active zone proteins. Nat Neurosci. 2012; 15(2):234–42. https://doi.org/10.1038/nn.2991 PMID: 22231427; PubMed Central PMCID: PMCPMC3848868.

55. Green JB, Gardner CD, Wharton RP, Aggarwal AK. RNA recognition via the SAM domain of Smaug. Mol Cell. 2003; 11(6):1537–48. PMID: 12820967.

56. Qiao F, Bowie JU. The many faces of SAM. Sci STKE. 2005;2005(286):re7. https://doi.org/10.1126/stke.2862005re7 PMID: 15928333.

57. Burnett PE, Blackshaw S, Lai MM, Qureshi IA, Burnett AF, Sabatini DM, et al. Neurabin is a synaptic protein linking p70 S6 kinase and the neuronal cytoskeleton. Proc Natl Acad Sci U S A. 1998; 95 (14):8351–6. Epub 1998/07/08. PMID: 9653190; PubMed Central PMCID: PMC20979.

58. Xu Y, Taru H, Jin Y, Quinn CC. SYD-1C, UNC-40 (DCC) and SAX-3 (Robo) function interdependently to promote axon guidance by regulating the MIG-2 GTPase. PLoS Genet. 2015; 11(4):e1005185. https://doi.org/10.1371/journal.pgen.1005185 PMID: 25876065; PubMed Central PMCID: PMCPMC4398414.

59. Nakanishi H, Obaishi H, Satoh A, Wada M, Mandai K, Satoh K, et al. Neurabin: a novel neural tissue-specific actin filament-binding protein involved in neurite formation. J Cell Biol. 1997; 139(4):951–61. PMID: 9362513; PubMed Central PMCID: PMCPMC2139968.

60. Orioli D, Colaluca IN, Stefanini M, Riva S, Dotti CG, Peverali FA. Rac3-induced neuritogenesis requires binding to Neurabin I. Mol Biol Cell. 2006; 17(5):2391–400. https://doi.org/10.1091/mbc.E05-08-0753 PMID: 16525025; PubMed Central PMCID: PMCPMC1446074.

61. Feng J, Yan Z, Ferreira A, Tomizawa K, Liauw JA, Zhuo M, et al. Spinophilin regulates the formation and function of dendritic spines. Proc Natl Acad Sci U S A. 2000; 97(16):9287–92. PMID: 10922077; PubMed Central PMCID: PMCPMC16860.

62. Causeret F, Jacobs T, Terao M, Heath O, Hoshino M, Nikolic M. Neurabin-I is phosphorylated by Cdk5: implications for neuronal morphogenesis and cortical migration. Mol Biol Cell. 2007; 18(11):4327–42. https://doi.org/10.1091/mbc.E07-04-0372 PMID: 17699587; PubMed Central PMCID: PMCPMC2043560.

63. Penzes P, Johnson RC, Sattler R, Zhang X, Huganir RL, Kambampati V, et al. The neuronal Rho-GEF Kalirin-7 interacts with PDZ domain-containing proteins and regulates dendritic morphogenesis. Neuron. 2001; 29(1):229–42. PMID: 11182094.

64. Ryan XP, Alldritt J, Svenningsson P, Allen PB, Wu GY, Nairn AC, et al. The Rho-specific GEF Lfc interacts with neurabin and spinophilin to regulate dendritic spine morphology. Neuron. 2005; 47(1):85–100. https://doi.org/10.1016/j.neuron.2005.05.013 PMID: 15996550.

65. Brenner S. The genetics of Caenorhabditis elegans. Genetics. 1974; 77(1):71–94. PMID: 4366476

66. Alvarez-Saavedra E, Horvitz HR. Many families of C. elegans microRNAs are not essential for development or viability. Curr Biol. 2010; 20(4):367–73. https://doi.org/10.1016/j.cub.2009.12.051 PMID: 20096582; PubMed Central PMCID: PMCPMC2844791.

67. Mello CC, Kramer JM, Stinchcomb D, Ambros V. Efficient gene transfer in C.elegans: extrachromosomal maintenance and integration of transforming sequences. Embo J. 1991; 10(12):3959–70. PMID: 1935914

68. Lucato CM, Halls ML, Ooms LM, Liu HJ, Mitchell CA, Whisstock JC, et al. The Phosphatidylinositol (3,4,5)-Trisphosphate-dependent Rac Exchanger 1.Ras-related C3 Botulinum Toxin Substrate 1 (P-Rex1.Rac1) Complex Reveals the Basis of Rac1 Activation in Breast Cancer Cells. J Biol Chem. 2015; 290(34):20827–40. https://doi.org/10.1074/jbc.M115.660456 PMID: 26112412; PubMed Central PMCID: PMCPMC4543645.